Microneedle Biosensor for Real-Time Electrical Detection of Nitric Oxide for In Situ Cancer Diagnosis During Endomicroscopy

*Do Hee Keum, Ho Sang Jung, Taejun Wang, Myeong Hwan Shin, Young-Eun Kim, Ki Hean Kim, G-One Ahn, and Sei Kwang Hahn**

Microneedle sensors (MSs) have attracted a great attention for simple, rapid, painless, noninvasive and transdermal sensing of biomarkers by puncturing the epithelial tissues such as stratum corneum and intestinal epithelium, and then analyzing biomarkers in the interstitial fluid of the body.[1–3] Microneedle arrays were modified with functional materials for the continuous real-time electrical detection of biomarkers for diagnostic applications.[4–6] Currently, there are only very few reports on the MS systems for in situ detection of biomarkers in internal organs. The most common and effective diagnostic system for internal organs is endomicroscopy, being widely used for the prevention, early detection and diagnosis of cancers by visualizing suspicious lesions that are typically inaccessible by other means.[7–9] However, it can only identify microscopic pathological features and often requires biopsy sampling of suspicious lesions for additional histopathological examination of cancers.

Nitric oxide (NO) is a potential clinical indicator for cancer progression.[10] Neuronal NO synthase (NOS) and endotherial NOS produce picomolar to nanomolar NO in various cell types to modulate anti-inflammatory responses.[11,12] Remarkably, micromolar NO is produced by inducible NOS (iNOS) in many types of inflammation-associated cancers.[13] The iNOS overexpressed in the early stage of cancers contributes to angiogenesis for further cancer growth.[14] The enhanced production of NO has previously been shown in melanoma model mice by electron paramagnetic resonance spectroscopy using an NO-trapping agent.[15] The iNOS expression in polyp regions of azoxymethane/dextran sulfate sodium (AOM/DSS)-induced colorectal cancer model mice is known to significantly increase compared to that in the surrounding normal tissues.[16–18] Previously, several electrochemical sensing systems made possible the real-time detection of NO with high sensitivity and specificity.[19,20] However, in these systems, it was difficult to detect physiologically relevant submicromolar concentrations of NO. Furthermore, they often required a large active area to harvest sufficient current for the electrochemical detection. To overcome this limitation, a field-effect transistor (FET) functionalized with specific binding molecules incorporating a gallium arsenide (GaAS) semiconductor has been fabricated for real-time electrical detection of NO.[21] Although this system could successfully detect the submicromolar concentrations of NO, the FET sensor using cytotoxic GaAs is not applicable to the clinic. GaAs has raised serious concerns about carcinogenicity to various organs including lung, testes, kidney, brain and immune systems.[22]

For the first time, we fabricated a MS at the end of an endomicroscope using polycarprolactone (PCL) micronoeedles coated with poly(3,4-ethylenedioxythiophene) (PEDOT) and then functionalized with hemin molecules on the surface for both endomicroscopic imaging and biosensing of colon cancer. Our MS demonstrated high carrier mobility for real-time, direct, continuous and rapid electrical read-out of NO signals with high sensitivity, selectivity, specificity, and stability. It was appropriate to detect sub-micromolar concentrations of NO in physiopathological conditions. In vitro electrical read-out of MS showed that the current gradually decreased in response to various concentrations of NO from chemical donors and macrophages. Our MS was rigid enough to penetrate melanoma mouse skin and rapidly distinguished the difference of NO concentrations between melanoma and normal tissues. In vivo application of MS together with white-light endomicroscopy provided not only identifying polyp regions in the colon but also detecting cancer-specific increase of NO production. This dual-diagnostic system can provide a powerful tool to effectively and rapidly diagnose cancers in patients.

Figure 1a shows a schematic illustration of MS fitted at the edge of endomicroscopic probe near a light source and a charge coupled device (CCD) camera for cancer imaging and diagnosis. MS with a dimension of 8 mm × 8 mm and a height of 700 μm was fabricated using PCL, which was rigid enough to penetrate the human tissues. PCL microneedle was surface modified with polydopamine (PD) for effective immobilization of PEDOT as a channel layer of electrochemical sensor, the latter of which was further complexed with hemin molecules by π–π interaction (Figure 1b). PD has been widely used to provide adhesion on the hydrophobic surface of polymers.[23] Meanwhile, PEDOT has superior conductivity, stability, and processability for channel fabrication in various fields.[24] PEDOT is composed of delocalized π electrons in thiophene rings of carbon backbones,

D. H. Keum, H. S. Jung, M. H. Shin, Prof. S. K. Hahn
Department of Materials Science and Engineering
Pohang University of Science and Technology (POSTECH), San 31
Hyoja-dong, Nam-gu, Pohang,
Kyungbuk 790–784, Korea
E-mail: skhanb@postech.ac.kr
T. Wang, Prof. K. H. Kim
Department of Integrative Biosciences and Biotechnology
POSTECH, 77 Cheongam-ro
Nam-gu, Pohang, Kyungbuk 790–784, Korea
Y. E. Kim, Prof. G.-O. Ahn
Department of Integrative Biosciences and Biotechnology
POSTECH, 77 Cheongam-ro
Nam-gu, Pohang, Kyungbuk 790–784, Korea

DOI: 10.1002/adhm.201500012

ADVANCED HEALTHCARE MATERIALS
www.advhealthmat.de

Materials Views
www.MaterialsViews.com

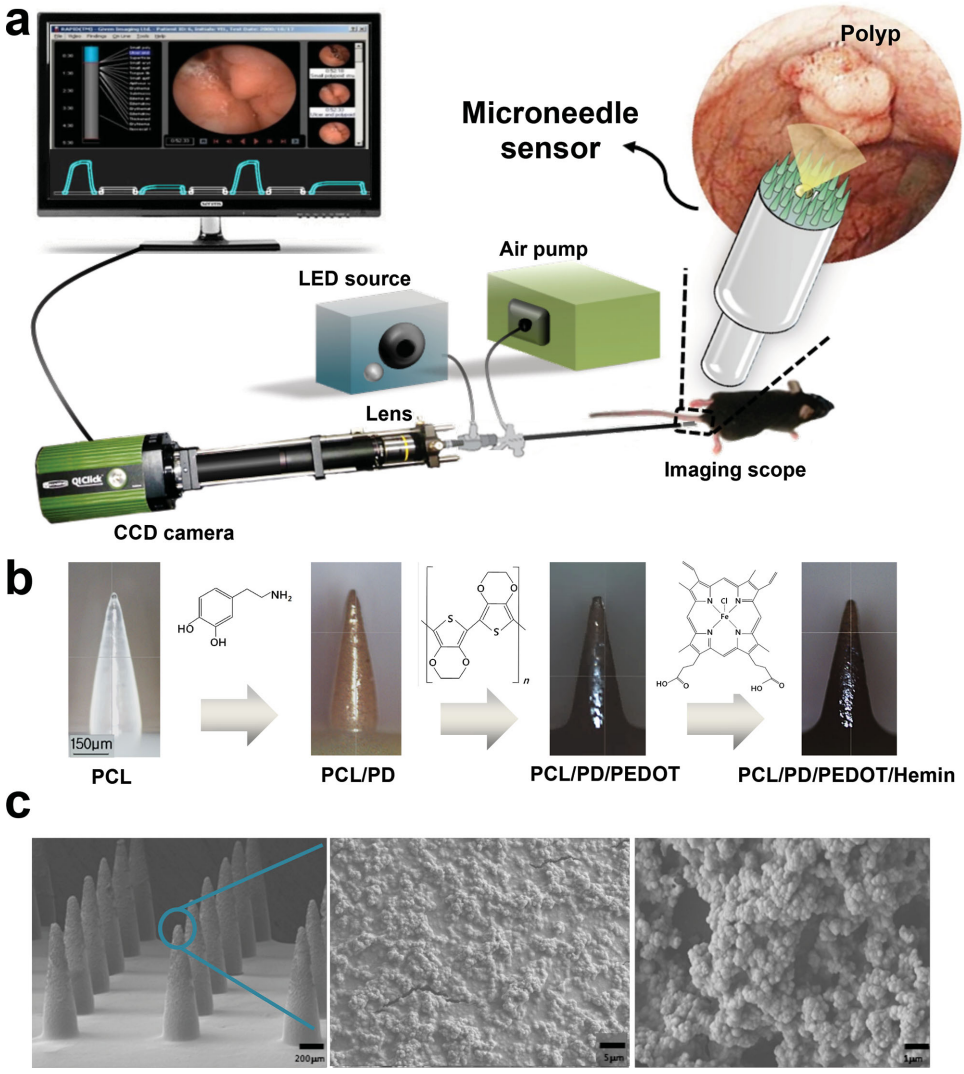

Figure 1. a) Schematic illustration of a microneedle sensor (MS) fabricated at the end of an endomicroscope for both imaging and sensing of cancer. b) Optical microscopic images of MS according to the fabrication process. c) Scanning electron microscopic images of MS and the enlarged images of a needle end point.

which have a high binding affinity to other π electrons of specific target molecules.[25] Hemin molecules also have extra π electrons in the center of the porphyrin ring and can form π–π interaction with PEDOT maintaining the electrical characteristics. This provides a *p*-type doping effect in the hole transport channel of PEDOT. As shown in Figure 1c, scanning electron microscopy (SEM) clearly showed the rough surface of PCL microneedle modified with PD, PEDOT, and hemin (PCL/PD/PEDOT/hemin). This system was successfully set for screening of tumor lesions by both intravital imaging and electrical detection of NO without the need of exogenous molecular labeling.

The molecule hemin is suitable for NO-targeting sensors because of its high binding constant and high affinity toward NO.[26] Energy-dispersive X-ray spectrometry (EDS) of MS showed a Fe peak of hemin molecules absorbed on the PEDOT layer around 6.4 eV, which indicated that Fe of hemin molecules was functionalized on the surface of MS (Figure S1a, Supporting Information). According to X-ray photoelectron spectroscopy (XPS), hemin-functionalized MS showed the presence of both $Fe2p_{1/2}$ and $Fe2p_{3/2}$ peaks around 710 eV and 725 eV, respectively (Figure S1b, Supporting Information). The peak of $Fe2p_{3/2}$ was much bigger than the peak of $Fe2p_{1/2}$ confirming that most of hemin molecules maintained the monomer form on the PEDOT.[27] Attenuated total reflectance–Fourier transform infrared spectroscopy (ATR-FTIR) of MS, which had not been functionalized with hemin, clearly showed the peaks of PEDOT only.[28,29] In case of hemin-functionalized MS, additional peaks were observed corresponding to C–O stretching vibration of carboxyl groups (1284 cm^{-1}) and C=O stretching vibration of amide groups (1621 cm^{-1}), all of which were in hemin molecules (Figure S1c, Supporting Information).[30] Raman spectrum of bare PEDOT showed oxyethylene ring deformation (985 cm^{-1}), C–O–C deformation (1100 cm^{-1}), Cα–Cα inter-ring stretching (1256 cm^{-1}), Cβ–Cβ stretching (1365 cm^{-1}), and symmetric (1429 cm^{-1}) and asymmetric (1500 cm^{-1}) C=C stretching (Figure S1d, Supporting

DOI: 10.1002/adhm.201500012

Information).[31] After hemin functionalization on PEDOT, several new bands were observed for the ν_{21} vibration mode of C_mH (1317 cm^{-1}), asymmetric stretching of C–C band (1562 cm^{-1}), and ν_{10} vibration mode of $C\alpha$–C_m (1,623 cm^{-1}) in hemin molecules.[32,33] These results of Raman spectrum of PEDOT before and after hemin functionalization confirmed the successful immobilization of hemin on the PEDOT. Considering the size of hemin molecule around 0.8 nm^2 and the quantified amount of hemin bound to the PEDOT channel, we could estimate that hemin molecules were functionalized as a monolayer by π–π conjugation.

In addition, cyclic voltammetry (CV) measurements showed that hemin-functionalized MS (PCL/PD/PEDOT/hemin) had well-defined and *quasi*-reversible redox peaks at –0.6 V and –0.4 V, representing Fe(III)/Fe(II) redox couples of hemin molecules (Figure S2a, Supporting Information). Electrochemical impedance spectroscopy (EIS) showed that the impedance of nonconductive PCL and PCL/PD, and PCL/PD/PEDOT was > 4.9 kΩ and 3.8 kΩ, and > 2.1 kΩ, respectively. While PEDOT separated the redox probe from the electrode surface, PCL/PD/PEDOT/hemin showed a small semicircle with a resistance of about 0.45 kΩ at high frequencies indicating that hemin molecules could reduce the interfacial resistance by effectively transporting charge carriers through reversible redoxing process of Fe(III)/Fe(II) (Figure S2b, Supporting Information). The electrocatalytic properties of hemin molecules to reduce NO were also investigated by CV and amperometric measurements (Figure S2c, Supporting Information). The results demonstrated that hemin-functionalized MS had a specific binding affinity and a high electrocatalytic activity toward NO. When we performed the real-time electrical detection of NO by using diethylamine NONOate sodium in phosphate buffer saline (PBS) at concentrations of 1×10^{-6}, 2×10^{-6}, 4×10^{-6}, 8×10^{-6}, and 16×10^{-6} M, we observed that the current of MS decreased as NO concentration increased (Figure S2d, Supporting Information). In contrast, MS without hemin did not respond to any of the tested NO concentrations.

To further assess the selectivity of MS toward NO in more biologically relevant system, we first used Dulbecco's modified Eagle medium (DMEM), a typical cell culture medium containing various amino acids and inorganic salts, added with 10% serum proteins. MS showed stepwise decrease in signals upon the addition of NO (**Figure 2**a), suggesting that electrical signals were not interfered by biological macromolecules. The sensitivity of MS measured in PBS and DMEM was about 1.56 μA cm^{-2} μM^{-1} and 1.44 μA cm^{-2} μM^{-1}, respectively. Furthermore, other potentially interfering biomolecules such as bovine serum albumin (BSA), glucose, galactose, Fe^{3+}, H_2O_2, ovalbumin, or lysozyme caused no significant current changes of MS (Figure 2b). However, current decline was only observed when NO was added at concentrations of 1×10^{-6} and 2×10^{-6} M, indicating an excellent selectivity of MS for NO. The current drop of MS might be due to the electron donation of NO to hemin molecules. Overall, these results suggest that MS

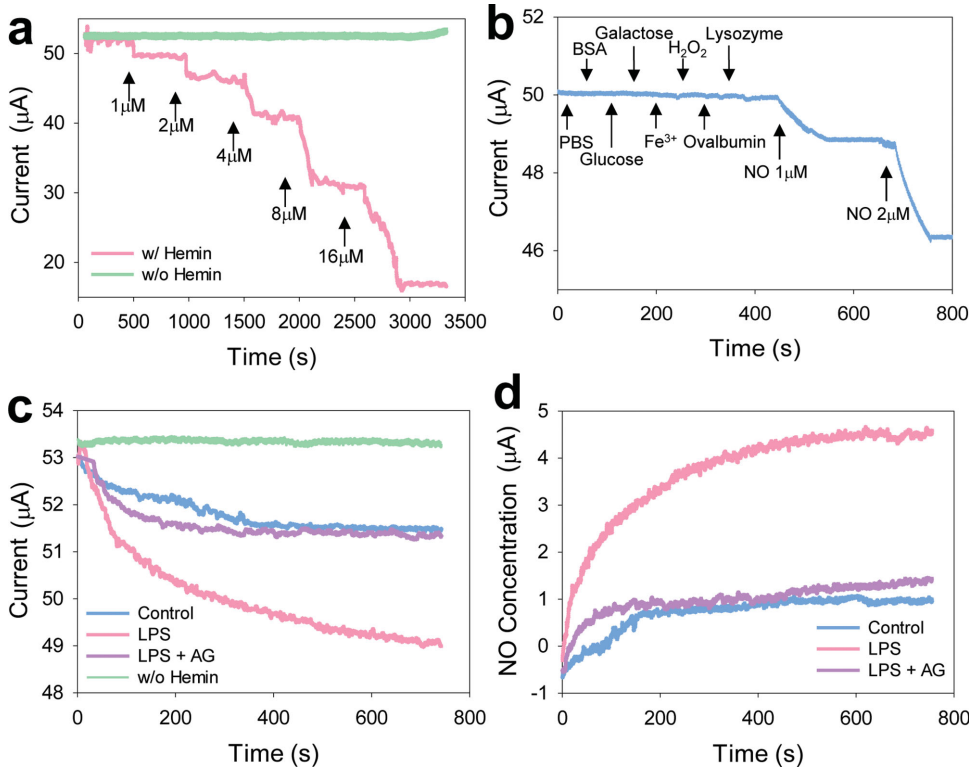

Figure 2. a) Real-time electrical detection of various concentrations of NO in DMEM using a microneedle sensor (MS) with and without hemin molecules. b) Selectivity of MS to a series of control solutions and NO solutions (1 and 2×10^{-6} M). c) Real-time electrical detection of NO from RAW 264.7 cells seeded on MS after treatment with none, 500 ng mL^{-1} of lipopolysaccharide (LPS), 500 ng mL^{-1} of LPS and 100×10^{-3} M of aminoguanidine (AG), and the MS without hemin. d) The converted concentration of NO from living cells treated with none, 500 ng mL^{-1} of LPS, and 500 ng mL^{-1} of LPS and 100×10^{-3} M of AG.

has a high sensitivity and selectivity toward NO in biologically relevant solution (Figure S3, Supporting Information).

We then performed in vitro real-time electrical detection of NO using a RAW 264.7 macrophage cell line. We treated these cells with lipopolysaccharide (LPS) for the activation of macrophages to produce NO via iNOS expression. MS could detect the generation of NO by iNOS (Figure S4a, Supporting Information). Also, MS could detect the suppression of NO production in the presence of an iNOS inhibitor, aminoguanidine (AG)[34] (Figure S4b, Supporting Information). As shown in Figure 2c, the electrical read-out of MS for LPS-treated cells decreased gradually in accordance with the increase of NO concentration, whereas the current change of MS was reduced and maintained after treatment with LPS (500 ng mL^{-1}) and AG (100×10^{-3} M). The current read-out of MS was converted to NO concentration using the calibration curve of Griess reagent test (Figure 2d). The overall concentrations of NO with appropriate time response were within the expected ranges of NO generated by RAW 264.7 cells.[35,36] These results therefore indicate a feasibility of MS for in vitro real-time monitoring of NO generated by RAW 264.7 cells.

Before in vivo electrical detection of NO, the cytotoxicity of materials used in MS was evaluated by MTT assay, which confirmed the biocompatibility of MS materials (Figure S5, Supporting Information). The MS had good mechanical properties and rigid enough to penetrate epidermis layer and reach to melanoma tissues (Figure S6, Supporting Information). Histological analysis with hematoxylin and eosin (H&E) staining revealed that MS was penetrated deep enough to sense NO in a melanoma tissue environment (**Figure 3**a and Figure S7, Supporting Information). To test whether MS can distinguish normal and melanoma tissues based on NO contents, we first measured NO levels in normal and melanoma tissues using Griess reagent kits. We observed that NO levels were two times higher in melanoma tissues compared to those in normal tissues (Figure 3b). Upon applying MS on the mouse skin bearing melanoma, in vivo electrical read-out of MS had an average current drop of 8.34 ± 0.16 μA, whereas that of MS applied on normal mouse skin had an average current drop of 3.26 ± 0.11 μA (Figure 3c). This difference indicates that MS is able to detect higher amount of NO in melanoma than the normal tissue, in consistent with already well-documented biological findings.[37,38] When MS was not functionalized with hemin molecules, the current drop of MS was similar between normal (3.09 ± 0.09 μA) and melanoma (2.94 ± 0.11 μA) tissues. Repeated in vivo application of MS to normal and melanoma tissues showed that the current drop could be fluctuated according to the type of tissues as we expected (Figure 3d).

We then combined MS with a lab-made endomicroscope for in vivo diagnosis of colon carcinoma. AOM/DSS-induced colorectal cancer model mice generate microadenomas polyps in colon, which gradually grow to macroscopic adenomas, adenomatous polyps, and finally adenocarcinomas via the inflammation-associated cancer progression.[39] Colon cancer was first screened by the white-light endomicroscopy, which clearly distinguished polyp regions from the normal tissue (**Figure 4**a,b). Histological analysis with H&E staining confirmed adenocarcinoma type of cancerous tissues (Figure 4c–e). To assess in vivo applicability, we applied the MS on those polyps. The current decreased with an average

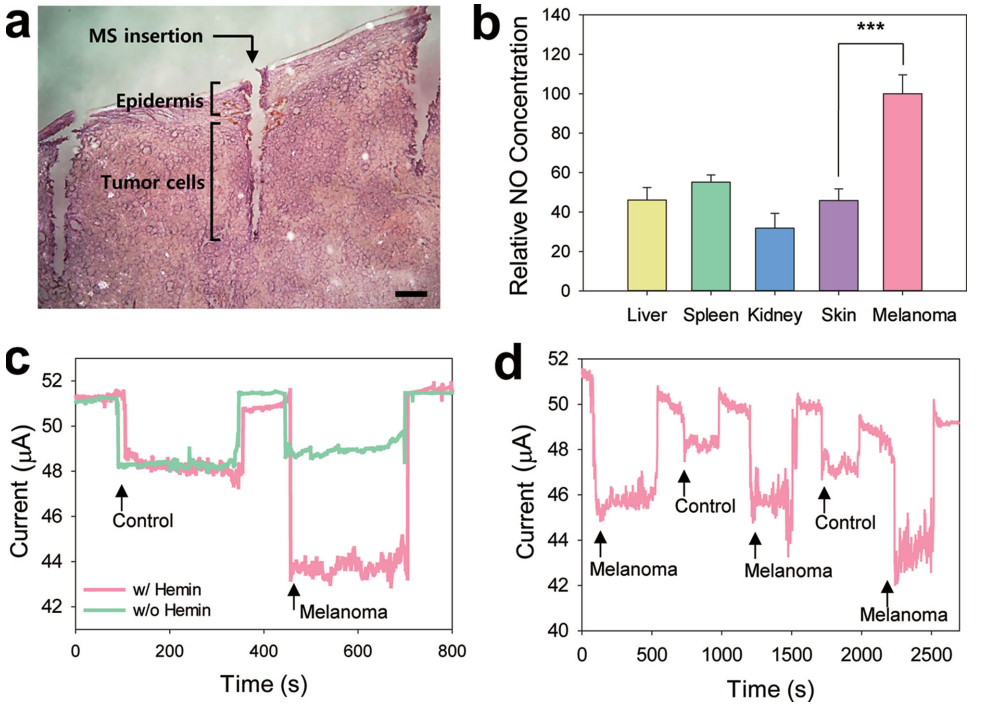

Figure 3. a) Histological analysis of melanoma tissue with H&E staining after insertion of a microneedle sensor (MS, scale bar = 100 μm). b) The relative concentration of NO released from normal and melanoma tissues by the analysis with Griess reagent kits (***$P < 0.001$). c) In vivo real-time electrochemical detection of NO released from melanoma tissues using MS with and without hemin molecules after insertion to normal and melanoma mouse skins. d) In vivo electrical read-out of current change of MS in normal and melanoma mouse skins alternately.

Adv. Healthcare Mater. **2015**,
DOI: 10.1002/adhm.201500012

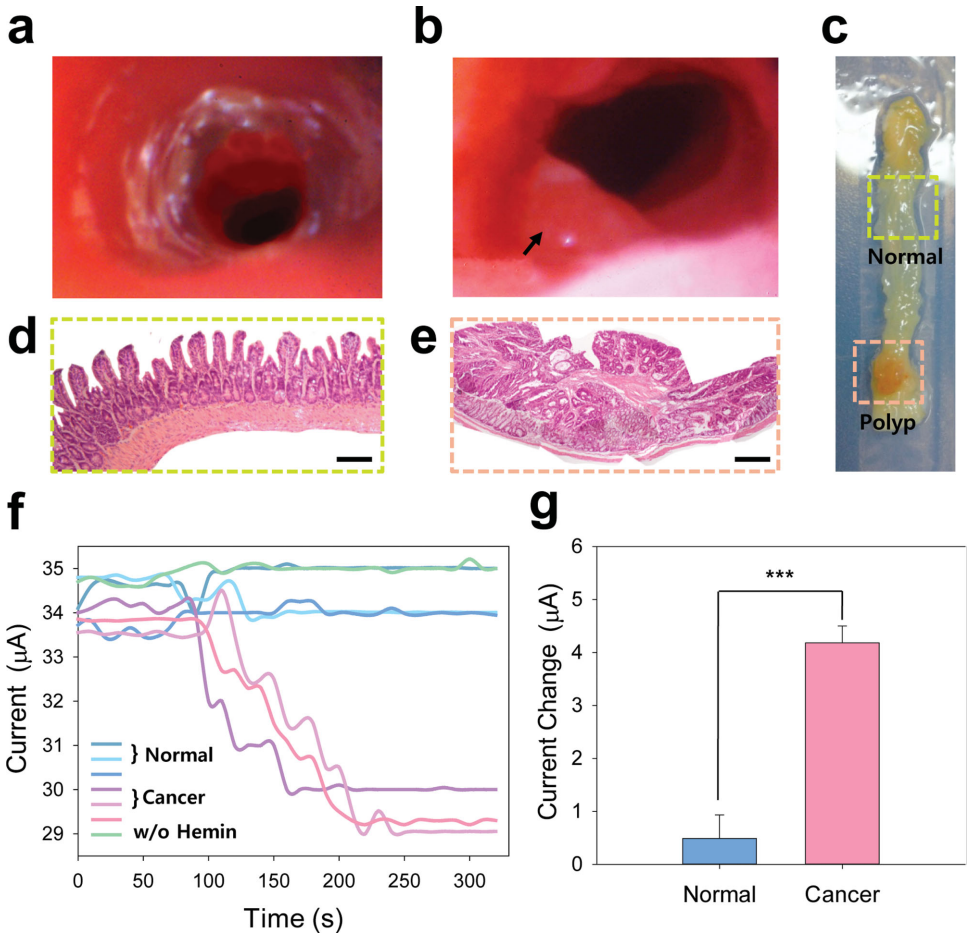

Figure 4. Real-time intravital endomicroscopic imaging of a) normal and b) AOM/DSS mouse colons. c) The photoimage of a fresh biopsied colonic tissue with normal and polyp regions. Histological images of d) normal and e) polyp regions of colons with H&E staining (scale bar = 150 μm). f) In vivo real-time electrical detection of NO in normal and polyp regions. g) The current change of MS applied on normal and polyp regions (***$P < 0.001$).

value of 4.12 ± 0.38 μA, whereas no obvious current change was observed in the normal region of colon (Figure 4f,g), suggesting that MS detected micromolar concentrations of NO produced in polyps. MS without hemin molecules showed no current change, in consistent with our in vitro results. Taken together, the dual-diagnostic system of endomicroscope and MS could effectively distinguish inflammation associated NO-rich cancer progression regions from normal regions in vivo with a high spatiotemporal resolution.

In conclusion, we successfully developed a new MS fitted on an endomicroscope for real-time electrical detection of NO signals from cancerous tissues with high sensitivity, selectivity, specificity, and stability. Our MS being able to operate at 100 mV with a high sensitivity of 1.44 μA cm^{-2} μM^{-1} clearly suggests a feasibility as an in vivo minimally invasive sensor. MS showed high stability for repeated sensing of NO in physiological condition for more than several days with a detection limit of 1×10^{-6} M to distinguish normal and cancer tissues in vivo. The dual-diagnostic system of endomicroscope and MS demonstrated high-resolution imaging combined with real-time electrical detection of NO released from cancer tissues, which can be a new platform for easy, precise, rapid and accurate detection of cancers.

Experimental Section

Fabrication of Microneedle Array: PCL pellets (0.5 g, number average MW = 80 kD, Sigma–Aldrich) were melted in a microneedle mold at 160 °C under vacuum for 3 h. After cooling to room temperature, PCL microneedle was peeled from the mold and soaked in 2 mg mL^{-1} of dopamine hydrochloride (Sigma–Aldrich) dissolved in 10×10^{-3} M of Tris buffer (pH 8.5) overnight under constant shaking. The PEDOT channel was prepared by solvent casting the solution of PEDOT-polystyrene sulfonate on the microneedle.

Sensor Device Fabrication: Working electrode and counter electrode made of titanium (10 nm)–palladium (10 nm)–gold (100 nm) films were formed using e-beam lithography, vacuum metal deposition, and lift-off process. The addition of Pd between Ti and Au was important for a metal diffusion barrier layer. To miniaturize an electrochemical sensor with high accuracy, we integrated a refference electrode directly on the sensor with 200 nm of silver layer by selective deposition on the microneedle using a shadow mask. Then silver layer was uniformly chlorinated in 1 M KCl/HCl buffer solution with applied current of 1 μA for 1 min. In the following step, the PCL/PD/PEDOT microneedle was immersed in

1 mg mL^{-1} of hemin chloride/DMSO solution for π–π interaction for 12 h, rinsed with DMSO, isopropyl alcohol, and deionized water to wash away the unattached hemin molecules.

In Vitro Real-Time Electrical Detection of NO: All of the following electrical measurements were conducted using a probe station (Lakeshore M5VC, MS tech), a computer-controlled analogue-to-digital converter (6030E, National Instruments), and CV (Sp-200 Potentiostat, Bio-Logic) under ambient conditions. A constant potential 0.1 V vs Ag/AgCl were applied for steady-state amperometric current responses of MS. The active reaction area of MS was coupled with a PDMS microfluidic channel with a height of 3 mm and filled with PBS (0.1 M pH 7.4). Diethylamine NONOate sodium at various concentrations (1×10^{-6}, 2×10^{-6}, 4×10^{-6}, 8×10^{-6}, and 16×10^{-6} M) was used as a precursor to release NO and introduced into the PDMS channel. To investigate the selectivity and specificity of MS as a NO sensor, potentially interfering chemicals including PBS, BSA, glucose, galactose, Fe^{3+}, H_2O_2, ovalbumin, and lysozyme were prepared at a similar concentration range with the body fluid. For in vitro detection of NO from macrophage cells, RAW 264.7 cells were seeded at 5×10^5 cells mL^{-1} on MS within a PDMS channel and cultured at 37 °C in a 5% CO_2 incubator for 24 h.

In Vivo Real-Time Electrical Read-out of MS in Melanoma Model Mice: Non-invasive detection of NO was carried out using MS in both normal and melanoma mice. The mice were anesthetized by inhaling a mixture of isoflurane and oxygen, and restrained in caskets to prevent their motions during the measurement. The animal model preparation was performed with protocols approved by the institutional animal care and use committee (IACUC) of the Seoul Asan Hospital and bred at the animal facility of POSTECH Biotech Center under specific pathogen-free conditions.

Dual-Diagnostic System for Intravital Real-Time Cancer Detection in Colon Cancer Model Mice: AOM/DSS model mice (over 12 weeks old) were used for NO detection and intravital endomicroscopic imaging inside the mouse colon lumen. After anesthetization, the colon was washed with PBS to remove feces. MS was connected with a power supply (6.5 digit low-noise power source, Agilent) using a cupper wire and the endomicroscopic probe was located in the middle of MS. The white-light endomicroscope was inserted through the abdominal incision for endomicroscopic imaging and screening of polyps. The measurement of NO with the MS was performed in the intravital state.

Supporting Information

Supporting Information is available from the Wiley Online Library or from the author.

Acknowledgements

This research was supported by the MSIP (Ministry of Science, ICT and Future Planning), Korea, under the "IT Consilience Creative Program" (NIPA-2014-H0201–14–1001). This research was supported by a Mid-career Researcher Program through NRF grant funded by the MEST (No. 2012R1A2A2A06045773).

Received: January 6, 2015
Revised: February 4, 2015
Published online:

[1] M. A. Invernale, B. C. Tang, R. L. Yotk, L. Le, D. Y. Hou, D. G. Anderson, *Adv. Healthcare Mater.* **2014**, *3*, 338.
[2] P. R. Miller, X. Xiao, L. Brener, D. B. Burckel, R. Narayan, R. Polsky, *Adv. Healthcare Mater.* **2014**, *6*, 876.
[3] Y. Yoon, G. S. Lee, K. Yoo, J. B. Lee, *Sensors* **2013**, *13*, 16672.
[4] G. Zheng, F. Patolsky, Y. Cui, W. U. Wang, C. M. Lieber, *Nat. Biotechnol.* **2005**, *23*, 1294.
[5] S. Swain, S. Beg, A. Singh, C. N. Oatro, M. E. B. Rao, *Curr. Drug Delivery* **2011**, *8*, 456.
[6] D. V. McAllister, P. M. Wang, S. P. Davis, J. H. Park, P. J. Canatella, M. G. Allen, M. R. Prausnitz, *Proc. Natl. Acad. Sci. U.S.A.* **2003**, *100*, 13755.
[7] G. J. Tearney, M. E. Brezinski, B. E. Bouma, S. A. Boppart, C. Pitris, J. F. Southern, J. G. Fujimoto, *Science* **1997**, *276*, 2037.
[8] P. Kim, E. Chung, H. Yamashita, K. E. Hung, A. Mizoguchi, R. Kucherlapati, D. Fukumura, R. K. Jain, S. H. Yun, *Nat. Methods* **2010**, *7*, 303.
[9] G. Oh, E. Chung, S. H. Yun, *Opt. Fiber Technol.* **2013**, *19*, 760.
[10] C. E. Eyler, Q. Wu, K. Yan, J. M. Macswords, D. C. Militello, K. L. Misuraca, J. D. Lathia, M. T. Forrester, J. Lee, J. S. Stamler, S. A. Glodman, M. Bredel, R. E. Mclendon, A. E. Solan, A. B. Hjelmeland, G. N. Rich, *Cell* **2011**, *146*, 53.
[11] S. Moncada, R. M. J. Palmer, E. A. Higgs, *Pharmacol. Rev.* **1991**, *2*, 109.
[12] S. Chakrabarti, C. K. Chan, T. Jiang, S. T. Davidge, *J. Leukoc. Biol.* **2012**, *91*, 947.
[13] M. N. Njau, J. Jacob, *Nat. Immunol.* **2014**, *15*, 219.
[14] W. Xu, L. Z. Liu, M. Loizidou, M. Ahmed, I. G. Charles, *Cell Res.* **2002**, *12*, 311.
[15] H. H. Wang, A. R. Mcintosh, B. B. Hasinoff, E. S. Rector, N. Ahmed, D. M. Nance, F. W. Orr, *Cancer. Res.* **2000**, *60*, 5862.
[16] D. Fukumura, S. Kashiwagi, R. K. Jain, *Nat. Rev. Cancer.* **2006**, *6*, 521.
[17] S. Ambs, W. G. Merriam, M. O. Ogunfusika, W. P. Bennett, N. Ishibe, S. P. Hussain, E. E. Tzeng, D. A. Geller, T. R. Billar, C. C. Harris, *Nat. Med.* **1998**, *4*, 1371.
[18] T. A. Ullman, S. H. Itzkowitz, *Gastroenterology* **2011**, *140*, 1807.
[19] I. R. Davies, X. Zhang, *Meth. Enzymol.* **2008**, *436*, 63.
[20] B. J. Privett, J. H. Shin, M. H. Schoenfisch, *J. Chem. Soc.* **2010**, *39*, 1925.
[21] D. G. Wu, D. Cahen, P. Graf, R. Naaman, A. Nitzan, D. Shvarts, *Chem. Eur. J.* **2001**, *7*, 1743.
[22] E. M. Bomhard, S. M. Cohen, G. P. Gelbke, G. M. Williams, *Regul. Toxicol. Pharmacol.* **2012**, *64*, 77.
[23] W. B. Tasi, W. T. Chen, H. W. Chein, W. H. Kuo, M. J. Wang, *Acta Biomater.* **2011**, *7*, 4187.
[24] A. Kros, S. W. F. M. Hovell, N. A. J. M. Sommerdijk, R. J. M. Nolte, *Adv. Mater.* **2001**, *13*, 1555.
[25] M. Gross, D. C. Muller, H. Nothofer, U. Scherf, D. Neher, C. Vrauchle, K. Meerholz, *Nature* **2000**, *405*, 661.
[26] S. Jiang, R. Cheng, X. Wang, T. Xue, Y. Liu, A. Nel, Y. Huang, X. Duan, *Nat. Commun.* **2013**, *4*, 2225.
[27] Y. Li, Z. Huang, Y. Li, Y. Xu, Y. Wang, E. Zhu, X. Duan, Y. Huang, *Surf. Sci. Rep.* **2013**, *3*, 1787.
[28] M. Salsamendi, R. Marcilla, M. Dobbelin, D. Mecerreyes, C. Pozo-Gonzalo, J. A. Pomposo, R. Pacios, *Phys. Status Solidi* **2008**, *205*, 1451.
[29] L. Yue, S. Wang, X. Zhao, L. Zhang, *J. Mater. Chem.* **2012**, *22*, 1094.
[30] C. Xu, J. Li, X. Wang, J. Wang, L. Wan, T. Li, M. Zhang, X. Shang, Y. Yang, *Mater. Chem. Phys.* **2012**, *132*, 858.
[31] T. Lindfors, Z. A. Boeva, R. M. Latonen, *RSC Adv.* **2014**, *4*, 25279.
[32] J. Terner, V. Palaniappan, A. Gold, T. Weiss, M. M. Fitzgerald, A. M. Sullivan, C. M. Hosten, *J. Inorg. Biochem.* **2006**, *100*, 480.
[33] A. J. Hobro, A. Konishi, C. Coban, N. I. Smith, *Analyst* **2013**, *138*, 3927.
[34] H. Shaked, L. J. Hofseth, A. Chumanevich, A. A. Chumanevich, J. Wang, T. Wang, K. Raniguchi, M. Guma, S. Shenouda, H. Clevers, C. C. Harris, M. Karin, *Proc. Natl. Acad. Sci. U.S.A.* **2012**, *109*, 14007.
[35] W. Cha, Y. C. Tung, M. E. Meyerhoff, S. Takayama, *Anal. Chem.* **2010**, *82*, 3300.
[36] M. Pekarova, J. Kralova, L. Kubala, M. Ciz, A. Lojek, C. Gregor, J. Hrbac, *Anal. Chem.* **2009**, *394*, 1497.
[37] L. C. Godoy, C. T. M Anderson, R. Chowdhury, L. J. Trudel, G. N. Wogan, *Proc. Natl. Acad. Sci. U.S.A.* **2011**, *109*, 20373.
[38] K. Tanese, E. A. Grimm, S. Ekmekcioglu, *Int. J. Cancer.* **2011**, *131*, 891.
[39] M. D. Robertis, E. Massi, M. L. Poeta, S. Carotti, S. Morini, L. Cecchetelli, E. Signori, V. M. Fazio, *J. Carcinog.* **2011**, *10*, 9.